

**Electronic Supplementary Information for
Organometallic One-Pot Synthesis of ZnO Quantum Dots Coated by
Sulfoxides as L-Type Ligands**

Maria Jędrzejewska,^{a,b} Małgorzata Wolska-Pietkiewicz,^{a*} Zygmunt Drużyński,^a and Janusz Lewiński^{a,b*}

^a Faculty of Chemistry, Warsaw University of Technology, Noakowskiego 3, 00-664 Warsaw, Poland. E-mail: janusz.lewinski@pw.edu.pl

^b Institute of Physical Chemistry, Polish Academy of Sciences, Kasprzaka 44/52, 01-224 Warsaw, Poland

Table of contents

1.	Complementary characterization for neat DMF-processed ZnO QDs	S2
	Optical measurements – UV-Vis and photoluminescence (PL) spectroscopy	S2
	Transmission Electron Microscopy (TEM) examination	S2
	Dynamic Light Scattering (DLS) measurements	S2
	Fourier Transform Infrared (FTIR) spectroscopy	S3
	Thermogravimetric analysis (TGA)	S3
2.	Complementary characterization for neat DBSO-processed ZnO QDs	S4
	Optical measurements – UV-Vis and photoluminescence (PL) spectroscopy	S4
	Transmission Electron Microscopy (TEM) examination	S4
	Powder X-Ray Diffraction (PXRD) analysis	S4
	Dynamic Light Scattering (DLS) measurements	S5
	Thermogravimetric analysis (TGA)	S5
3.	Characterization of adduct-type [Et ₂ Zn(L)] precursors	S6
	Nuclear Magnetic Resonance (NMR) spectroscopy	S6
4.	Complementary characterization for ZnO QDs obtained through L-type protector-assisted synthesis	S9
	Optical measurements – UV-Vis and photoluminescence (PL) spectroscopy	S9
	Powder X-Ray Diffraction (PXRD) analysis	S10
	Calculated core sizes of ZnO-L QDs - summary	S10
	Shape analysis of ZnO QDs – 2D plots	S11
	Dynamic Light Scattering (DLS) analysis	S12
	Nuclear Magnetic Resonance (NMR) spectroscopy	S13
	Fourier Transform Infrared (FTIR) spectroscopy	S16
	Thermogravimetric analysis (TGA)	S20
5.	Additional information and calculations for TGA, DLS and optical data	S21
	Ligand content determined from TGA data	S21
	DLS results - summary	S23
	Optical measurements – summary	S23
6.	References	S23

1. Complementary characterization for neat DMF-processed ZnO QDs

Optical measurements – UV-Vis and photoluminescence (PL) spectroscopy

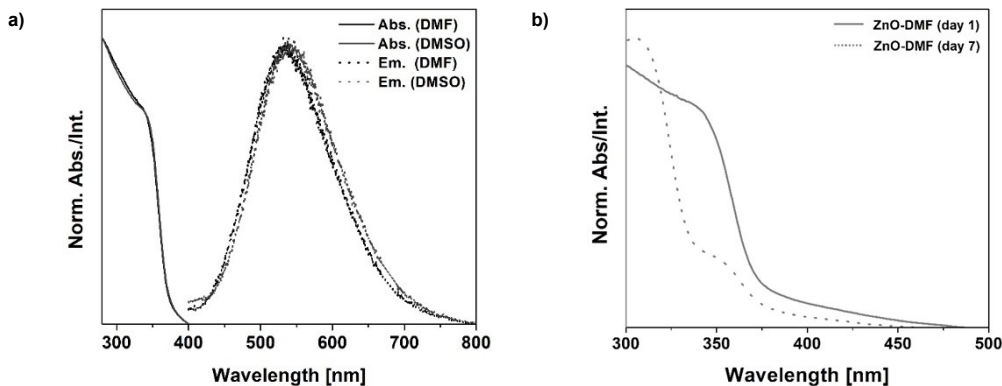


Figure S1. a) Normalized absorption (solid line) and emission spectra (dotted line) of as-prepared ZnO-DMF collected in DMF (black line) and in DMSO (grey line) solution; b) The absorption spectra of freshly prepared ZnO-DMF (solid line) and ZnO-DMF after 1 week of storage in DMF (dotted line).

Transmission Electron Microscopy (TEM) examination

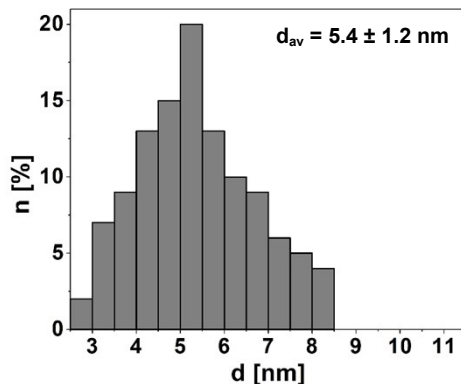


Figure S2. The size distribution of ZnO-DMF (based on the analysis of TEM images).

Dynamic Light Scattering (DLS) measurements

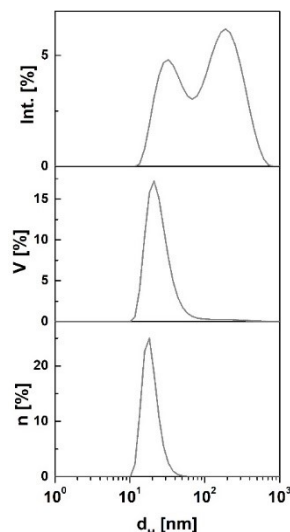


Figure S3. Intensity-averaged, volume-averaged and number-averaged size distribution of solvodynamic diameter of as-prepared ZnO-DMF obtained from the representative DLS measurements in DMF solution.

Fourier Transform Infrared (FTIR) spectroscopy

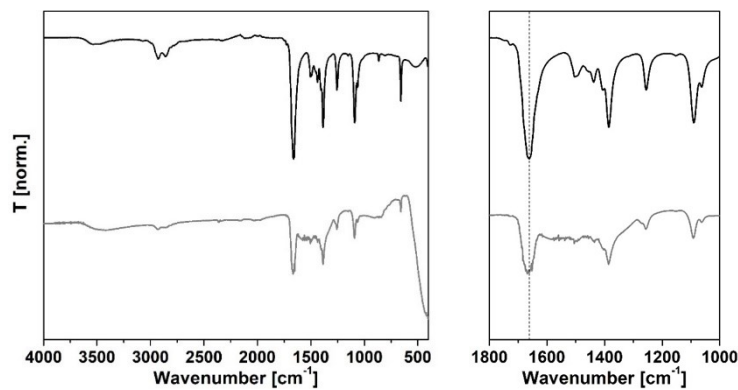


Figure S4. FTIR spectra of ZnO-DMF (grey line) and DMF (black line).

Thermogravimetric analysis (TGA)

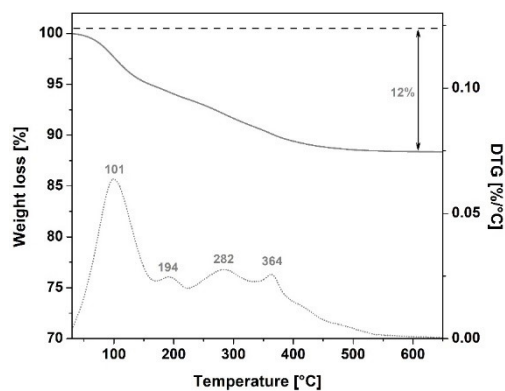


Figure S5. The TGA (solid line) and derivative thermogravimetric analysis (DTG) (dotted line) traces showing the decomposition of **ZnO-DMF** under synthetic air flow conditions.

2. Complementary characterization for neat DBSO-processed ZnO QDs

Optical measurements – UV-Vis and photoluminescence (PL) spectroscopy

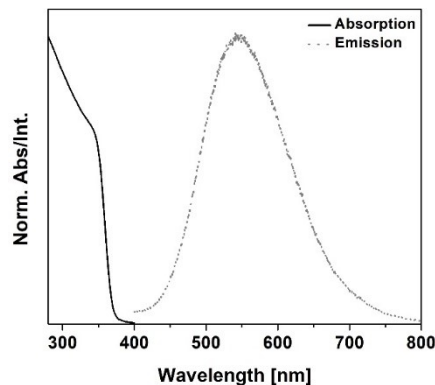


Figure S6. Normalized absorption (solid line) and emission spectra (dotted line) of as-prepared ZnO-DBSO collected in DMSO.

Transmission Electron Microscopy (TEM) examination

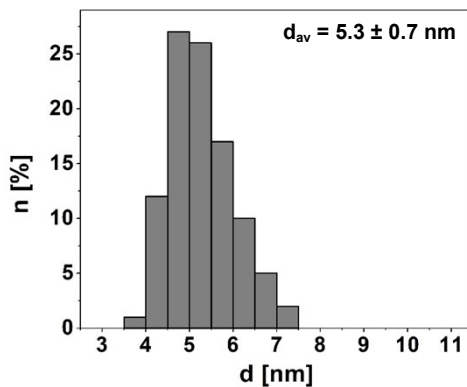


Figure S7. The size distribution of ZnO-DBSO (based on the analysis of TEM images).

Powder X-Ray Diffraction (PXRD) analysis

ZnO QDs' core size was calculated from the Scherrer's formula:

$$d_c = \frac{k \cdot \lambda}{\beta \cdot \cos \theta}$$

where:

d_c - diameter of ZnO QDs' core;

k - Scherrer's constant (shape factor), for sphere-like grains: $k=0.89$;

λ - the wavelength of X-rays, $\lambda = 1.54 \text{ \AA}$;

θ - Bragg diffraction angle;

β - is the full width at half-maximum (FWHM) of the diffraction peak corresponding to diffraction plane.

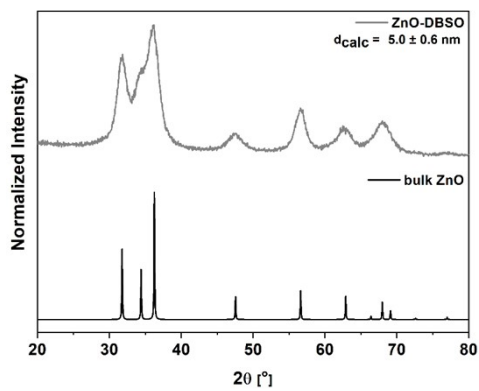


Figure S8. Powder X-ray diffraction pattern of ZnO-DBSO (grey line) in comparison with bulk ZnO pattern (black line) confirming wurtzite crystalline core structure.

Dynamic Light Scattering (DLS) measurements

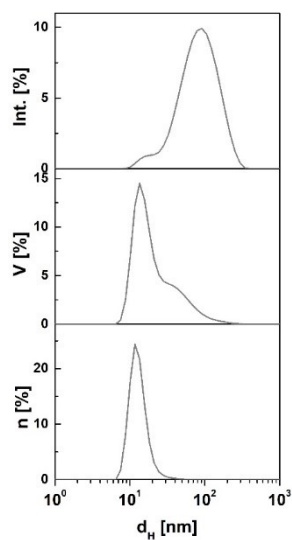


Figure S9. Intensity-averaged, volume-averaged and number-averaged size distribution of solvodynamic diameter of as-prepared ZnO-DBSO obtained from the representative DLS measurements in DMSO solution.

Thermogravimetric analysis (TGA)

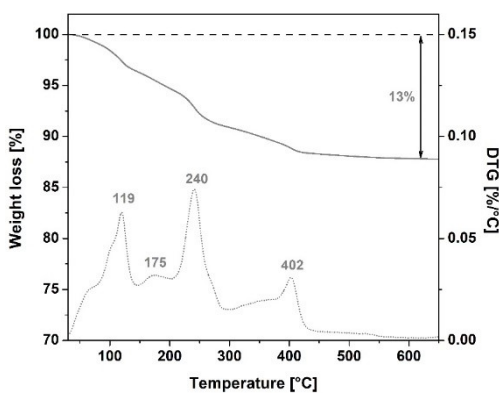


Figure S10. The TGA (solid line) and derivative thermogravimetric analysis (DTG) (dotted line) traces showing the decomposition of ZnO-DBSO under synthetic air flow conditions.

3. Characterization of adduct-type $[\text{Et}_2\text{Zn}(\text{L})]$ precursors

Nuclear Magnetic Resonance (NMR) spectroscopy

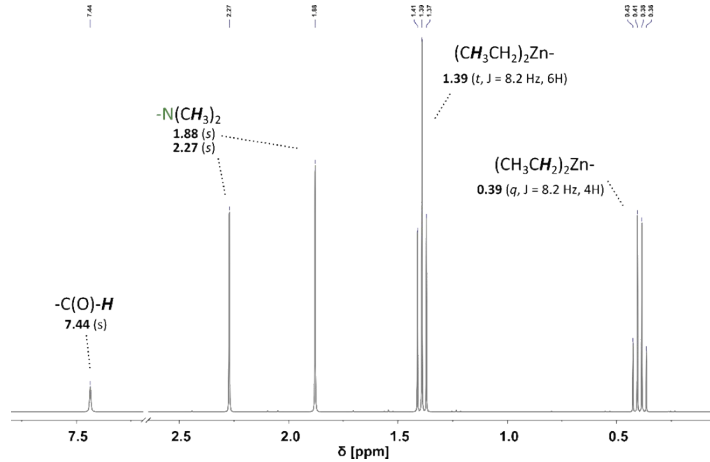


Figure S11. ^1H NMR spectra of $[\text{Et}_2\text{Zn}(\text{DMF})]$ in C_6D_6 .

[Et₂Zn(DMF)]: ^1H NMR (C_6D_6 , 400 MHz, 303 K): δ = 0.39 (q, $(\text{CH}_3\text{CH}_2)_2\text{Zn}-$), 1.39 (t, $(\text{CH}_3\text{CH}_2)_2\text{Zn}-$), 1.88 (s, $(\text{CH}_3)_2\text{N}-$), 2.27 (s, $(\text{CH}_3)_2\text{N}-$), 7.44 (s, -C(O)-H); ^{13}C NMR (C_6D_6 , 400 Hz, 303 K): δ = 5.41 ($(\text{CH}_3\text{CH}_2)_2\text{Zn}-$), 11.30 ($(\text{CH}_3\text{CH}_2)_2\text{Zn}-$), 30.74 ($(\text{CH}_3)_2\text{N}-$), 35.31 ($(\text{CH}_3)_2\text{N}-$), 162.57 (-C(O)-H) ppm.

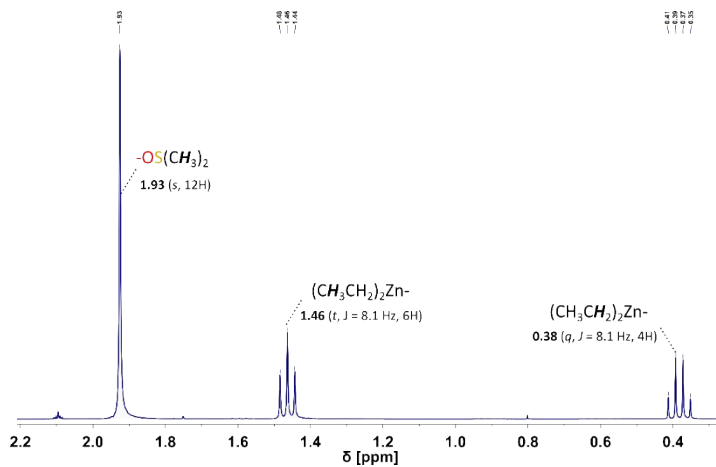


Figure S12. ^1H NMR spectra of $[\text{Et}_2\text{Zn}(\text{DMSO})]$ in toluene- d_8 .

[Et₂Zn(DMSO)]: ^1H NMR (toluene- d_8 , 400 MHz, 303 K): δ = 0.38 (q, $(\text{CH}_3\text{CH}_2)_2\text{Zn}-$), 1.46 (t, $(\text{CH}_3\text{CH}_2)_2\text{Zn}-$), 1.93 (s, $(\text{CH}_3)_2\text{SO}-$) ppm; ^{13}C NMR (toluene- d_8 , 400 MHz, 303 K): δ = 5.32 ($(\text{CH}_3\text{CH}_2)_2\text{Zn}-$), 12.44 ($(\text{CH}_3\text{CH}_2)_2\text{Zn}-$), 40.30 ($(\text{CH}_3)_2\text{SO}-$) ppm.

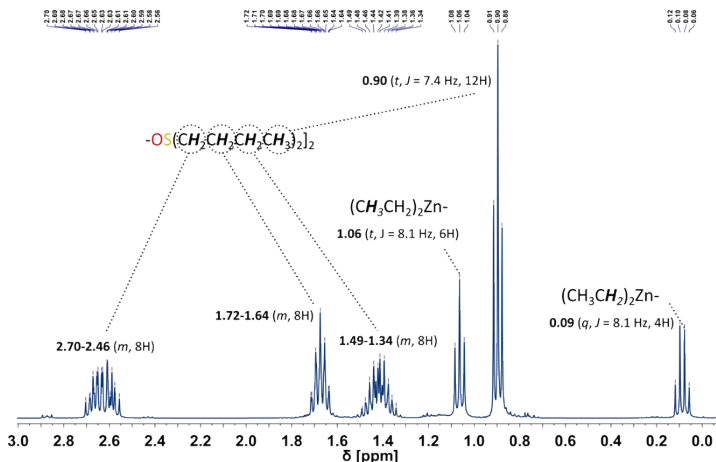


Figure S13. ^1H NMR spectra of $[\text{Et}_2\text{Zn(DBSO)}]$ in CDCl_3 .

[$\text{Et}_2\text{Zn(DBSO)}$]: ^1H NMR (CDCl_3 , 400 MHz, 303 K): δ = 0.09 (q, $(\text{CH}_3\text{CH}_2)_2\text{Zn}-$), 0.90 (t, $(\text{CH}_3\text{CH}_2\text{CH}_2\text{CH}_2)_2\text{SO}-$), 1.06 (t, $(\text{CH}_3\text{CH}_2)_2\text{Zn}$), 1.34-1.49 (m, $(\text{CH}_3\text{CH}_2\text{CH}_2\text{CH}_2)_2\text{SO}-$) 1.64-1.72 (m, $(\text{CH}_3\text{CH}_2\text{CH}_2\text{CH}_2)_2\text{SO}-$), 2.46-1.70 (m, $(\text{CH}_3\text{CH}_2\text{CH}_2\text{CH}_2)_2\text{SO}-$) ppm; ^{13}C NMR (CDCl_3 , 400 MHz, 303 K): δ = 5.58 ($(\text{CH}_3\text{CH}_2)_2\text{Zn}-$), 10.87 ($(\text{CH}_3\text{CH}_2)_2\text{Zn}-$), 13.57 ($(\text{CH}_3\text{CH}_2\text{CH}_2\text{CH}_2)_2\text{SO}-$), 21.98 ($(\text{CH}_3\text{CH}_2\text{CH}_2\text{CH}_2)_2\text{SO}-$), 24.54 ($(\text{CH}_3\text{CH}_2\text{CH}_2\text{CH}_2)_2\text{SO}-$), 51.80 ($(\text{CH}_3\text{CH}_2\text{CH}_2\text{CH}_2)_2\text{SO}-$) ppm.

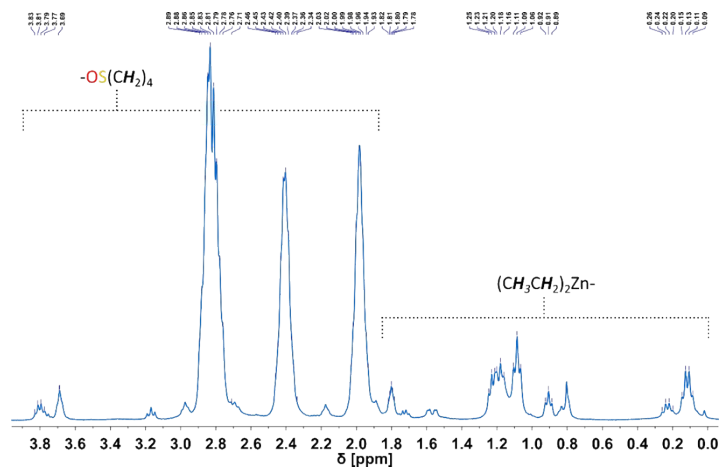


Figure S14. ^1H NMR spectra of $[\text{Et}_2\text{Zn(TMSO)}]$ in CDCl_3 .

[$\text{Et}_2\text{Zn(TMSO)}$]: ^1H NMR (CDCl_3 , 400 MHz, 303 K): δ = 0.12, 0.23 (q, $(\text{CH}_3\text{CH}_2)_2\text{Zn}$), 1.09, 1.20 (t, $\text{CH}_3\text{CH}_2)_2\text{Zn}$), 1.93-2.03, 2.34-2.46, 2.71-2.89 (m, - CH_2- groups); ^{13}C NMR (CDCl_3 , 400 MHz, 303 K): δ = 25.48, 54.46 ppm.

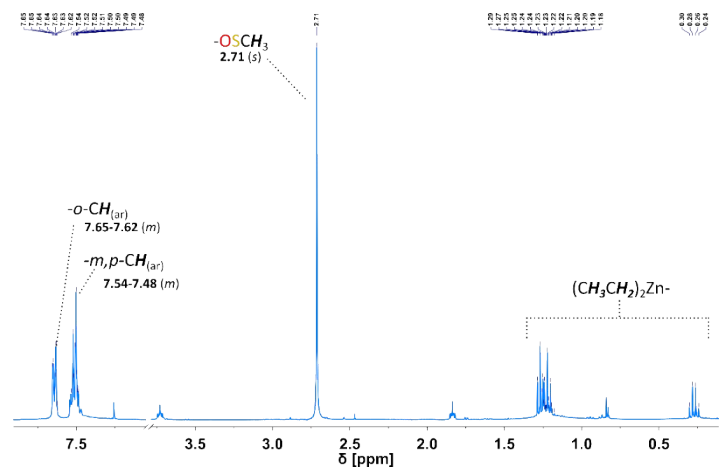


Figure S15. ^1H NMR spectra of $[\text{Et}_2\text{Zn(MPSO)}]$ in CDCl_3 .

[$\text{Et}_2\text{Zn(MPSO)}$]: ^1H NMR (CDCl_3 , 400 MHz, 303 K): δ = 0.27 (q, $(\text{CH}_3\text{CH}_2)_2\text{Zn}$), 1.18-1.29 (m, $(\text{CH}_3\text{CH}_2)_2\text{Zn}$), 2.71 (s, CH_3SO); 7.48-7.54 (m, - m,p - $\text{CH}_{(\text{ar})}$), 7.62-7.65 (m, - $\text{o-CH}_{(\text{ar})}$) ppm; ^{13}C NMR (CDCl_3 , 400 MHz, 303 K): δ = 1.14, ($(\text{CH}_3\text{CH}_2)_2\text{Zn}$), 13.27 ($(\text{CH}_3\text{CH}_2)_2\text{Zn}$), 43.85 (CH_3SO) 123.45 ($\text{o-CH}_{(\text{ar})}$), 129.30 ($m\text{-CH}_{(\text{ar})}$), 130.99 ($p\text{-CH}_{(\text{ar})}$), 145.60 ppm.

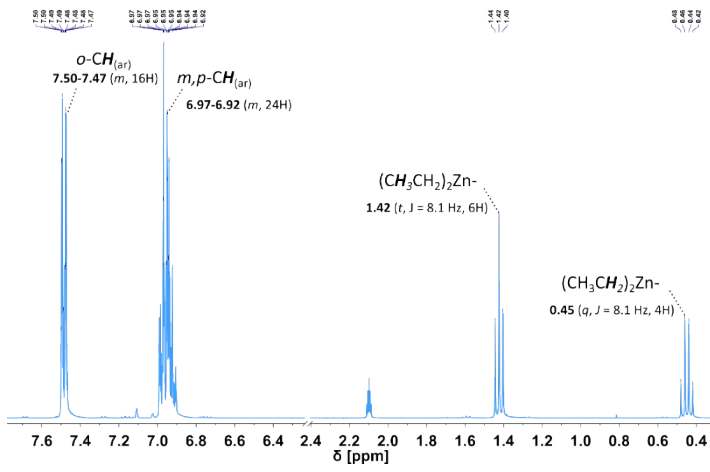


Figure S16. ^1H NMR spectra of $[\text{Et}_2\text{Zn}(\text{DPSO})]$ in toluene- d_6 .

[Et₂Zn(DPSO)]: ^1H NMR (toluene- d_6 , 400 MHz, 303 K): $\delta =$: $\delta = 0.45$ (q, $(\text{CH}_3\text{CH}_2)_2\text{Zn}$), 1.42 (t, $(\text{CH}_3\text{CH}_2)_2\text{Zn}$), 6.92 - 6.97 (m, -*m,p*-CH_(ar)), 7.50 - 7.47 (m, -*o*-CH_(ar)) ppm; ^{13}C NMR (toluene- d_6 , 400 MHz, 303 K): $\delta = 5.84$ ($(\text{CH}_3\text{CH}_2)_2\text{Zn}$), 11.70 ($(\text{CH}_3\text{CH}_2)_2\text{Zn}$)), 124.71 (*o*-CH_(ar)), 129.24 (*m*-CH_(ar)), 130.67 (*p*-CH_(ar)), 147.12 (-C_(ar)-SO) ppm.

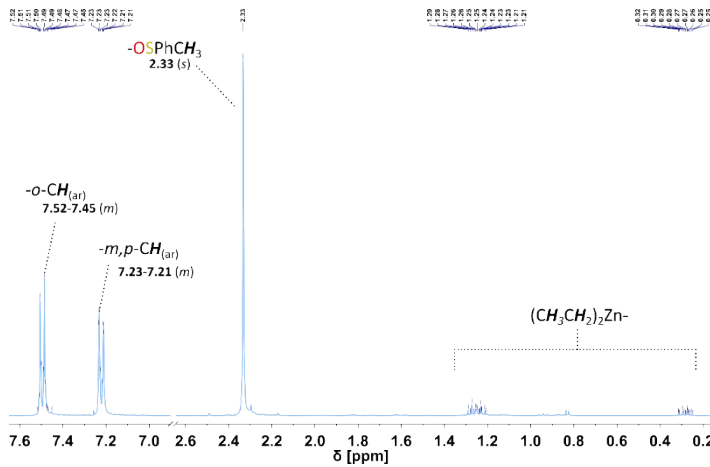


Figure S17. ^1H NMR spectra of $[\text{Et}_2\text{Zn}(\text{DTSO})]$ in CDCl_3 .

[Et₂Zn(DTSO)]: ^1H NMR (CDCl_3 , 400 MHz, 303 K): $\delta = 0.29$ (m, $(\text{CH}_3\text{CH}_2)_2\text{Zn}$), 1.25 (m, $(\text{CH}_3\text{CH}_2)_2\text{Zn}$), 2.33 (s, CH_3SO), 7.21 - 7.23 (m, -*m,p*-CH_(ar)), 7.45 - 7.52 (-*o*-CH_(ar)); ^{13}C NMR (CDCl_3 , 400 MHz, 303 K): $\delta = 21.34$ (CH_3Ph), 124.90 , 129.94 (*o*-CH_{ar}) (*m*-CH_(ar)), 141.44 (*p*-CH_(ar)), 142.51 (-C_(ar)) ppm

4. Complementary characterization for ZnO QDs obtained through L-type protector-assisted synthesis

Optical measurements – UV-Vis and photoluminescence (PL) spectroscopy

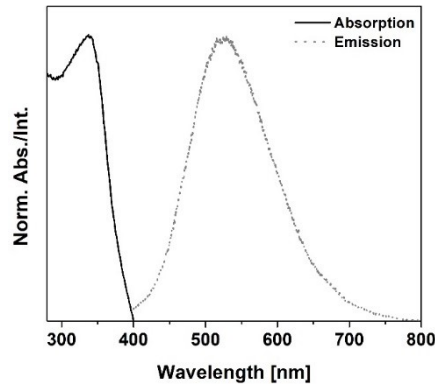


Figure S18. Normalized absorption (solid line) and emission spectra (dotted line) of prepared ZnO-DMF' QDs collected in DMSO.

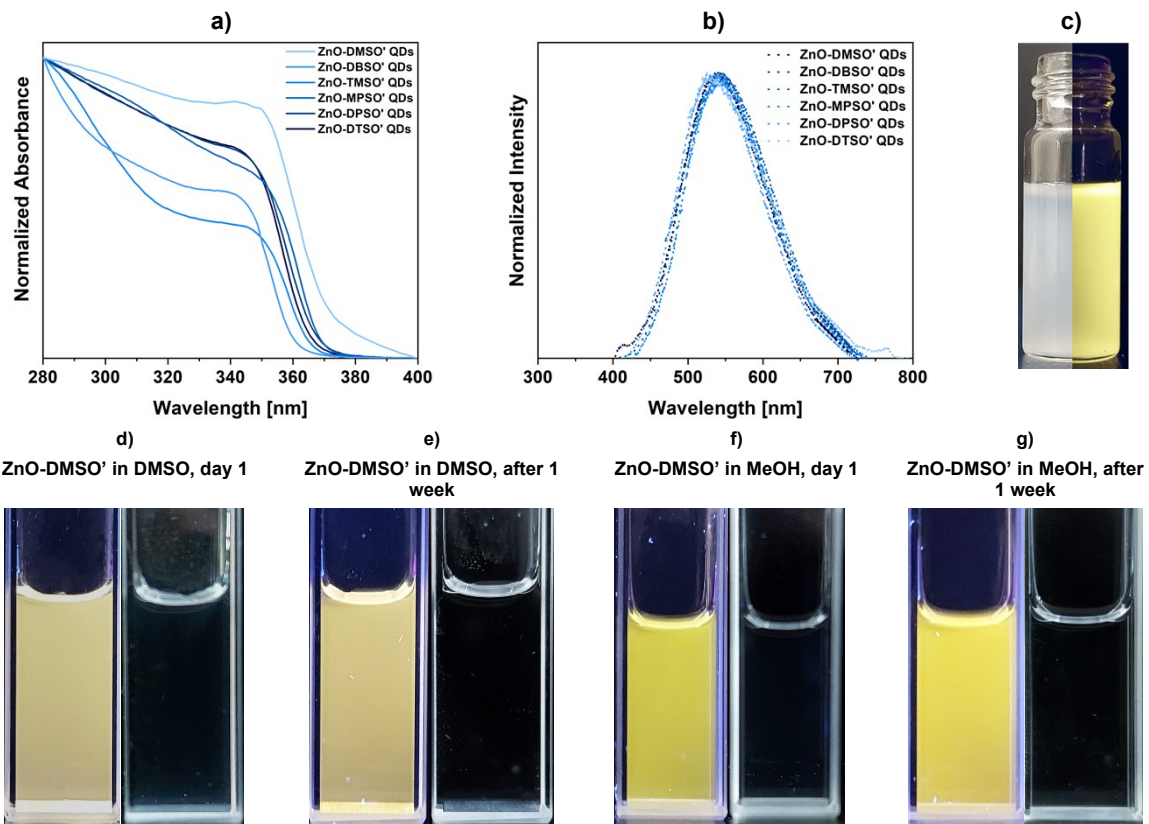


Figure S19. Normalized absorption (a) and emission (b) spectra of prepared ZnO-DMSO', ZnO DBSO', ZnO-TMSO', ZnO-MPSO', ZnO-DPSO', ZnO-DTSO' collected in DMSO and (c) photographs of ZnO-DMSO' suspension in DMSO (1 mg/mL) under visible and 365 nm UV light; the photographs of ZnO-DMSO' colloids under UV light (left) and under daylight (right) formed in DMSO (d – freshly filtered, e – after 1 week of storage) and in methanol (f – freshly filtered, g – after 1 week of storage), filtered through 0.45 µm PTFE syringe filter.

Powder X-Ray Diffraction (PXRD) analysis

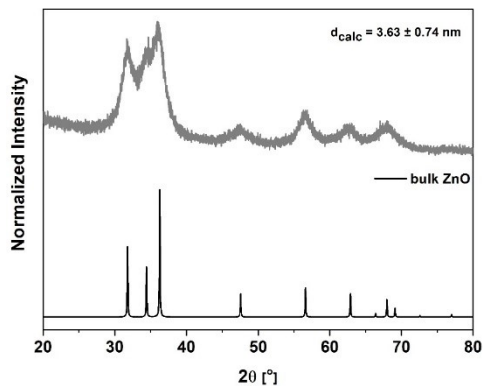


Figure S20. Powder X-ray diffraction pattern of ZnO-DMF' (grey line) in comparison with bulk ZnO pattern (black line) confirming wurtzite crystalline core structure.

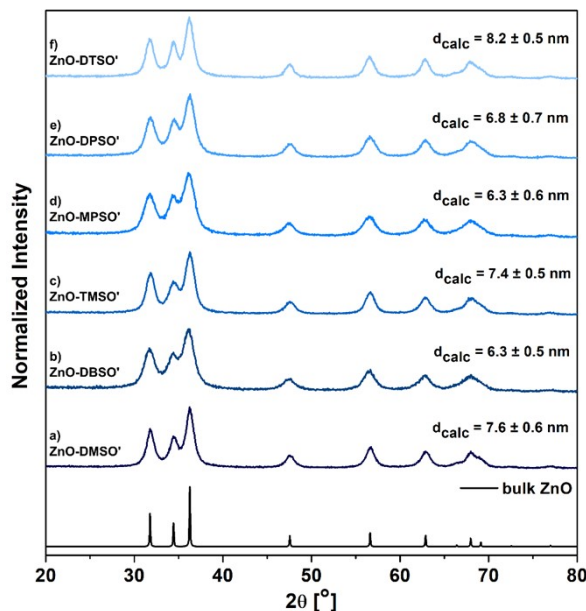


Figure S21. Powder X-ray diffraction patterns of a) ZnO-DMSO', b) ZnO DBSO', c) ZnO-TMSO', d) ZnO-MPSO', e) ZnO-DPSO', f) ZnO-DTSO' in comparison with bulk ZnO pattern (black line) confirming wurtzite crystalline core structure.

Calculated core sizes of ZnO-L QDs - summary

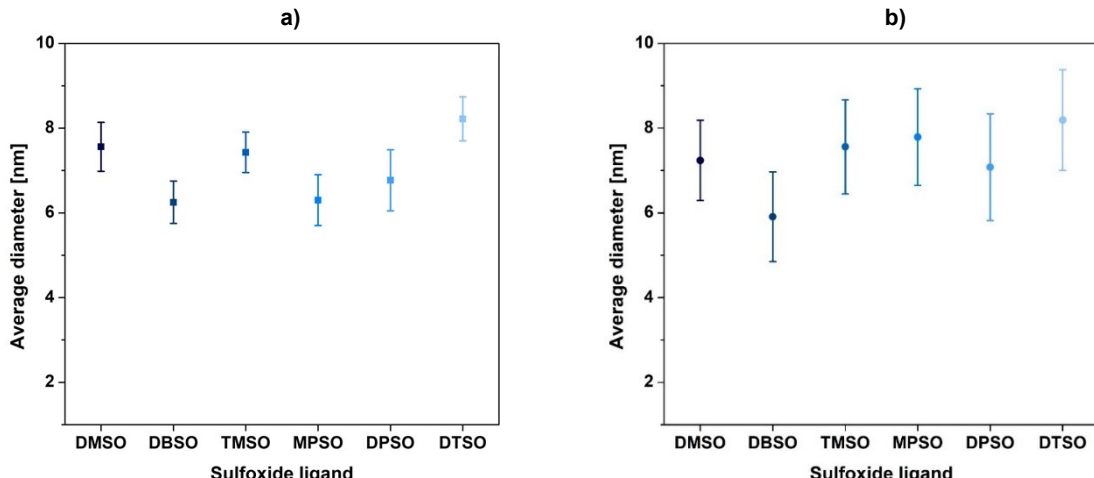


Figure S22. The representation of ligand-independent core size of the respective ZnO-DMSO', ZnO DBSO', ZnO-TMSO', ZnO-MPSO', ZnO-DPSO', ZnO-DTSO' derived from (a) PXRD and (b) TEM data.

Shape analysis of ZnO QDs – 2D plots

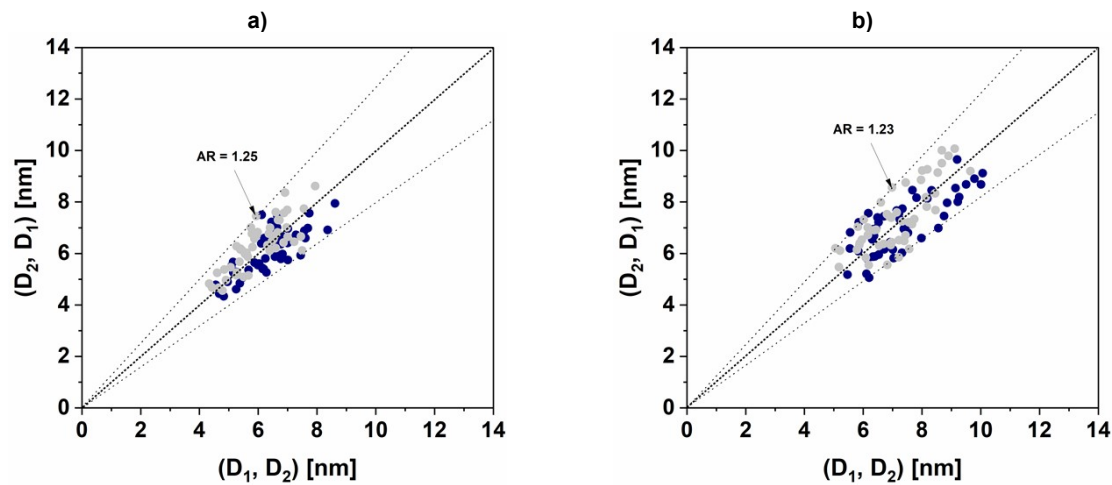


Figure S23. 2D plots of shape analysis for a) $\text{ZnO-DMSO}'$ and b) $\text{ZnO-DPSO}'$ derived from TEM data. Notations: D_1 – length, D_2 – width of QD.¹

Dynamic Light Scattering (DLS) analysis

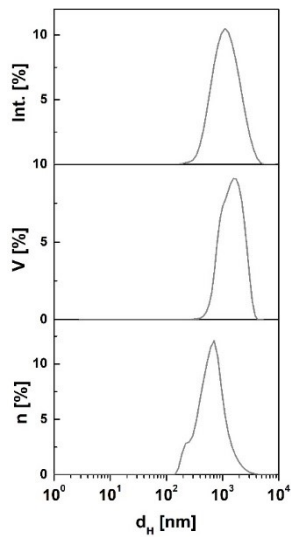


Figure S24. Intensity-averaged, volume-averaged and number-averaged size distribution of solvodynamic diameter of as-prepared **ZnO-DMF'** obtained from the representative DLS measurements in THF.

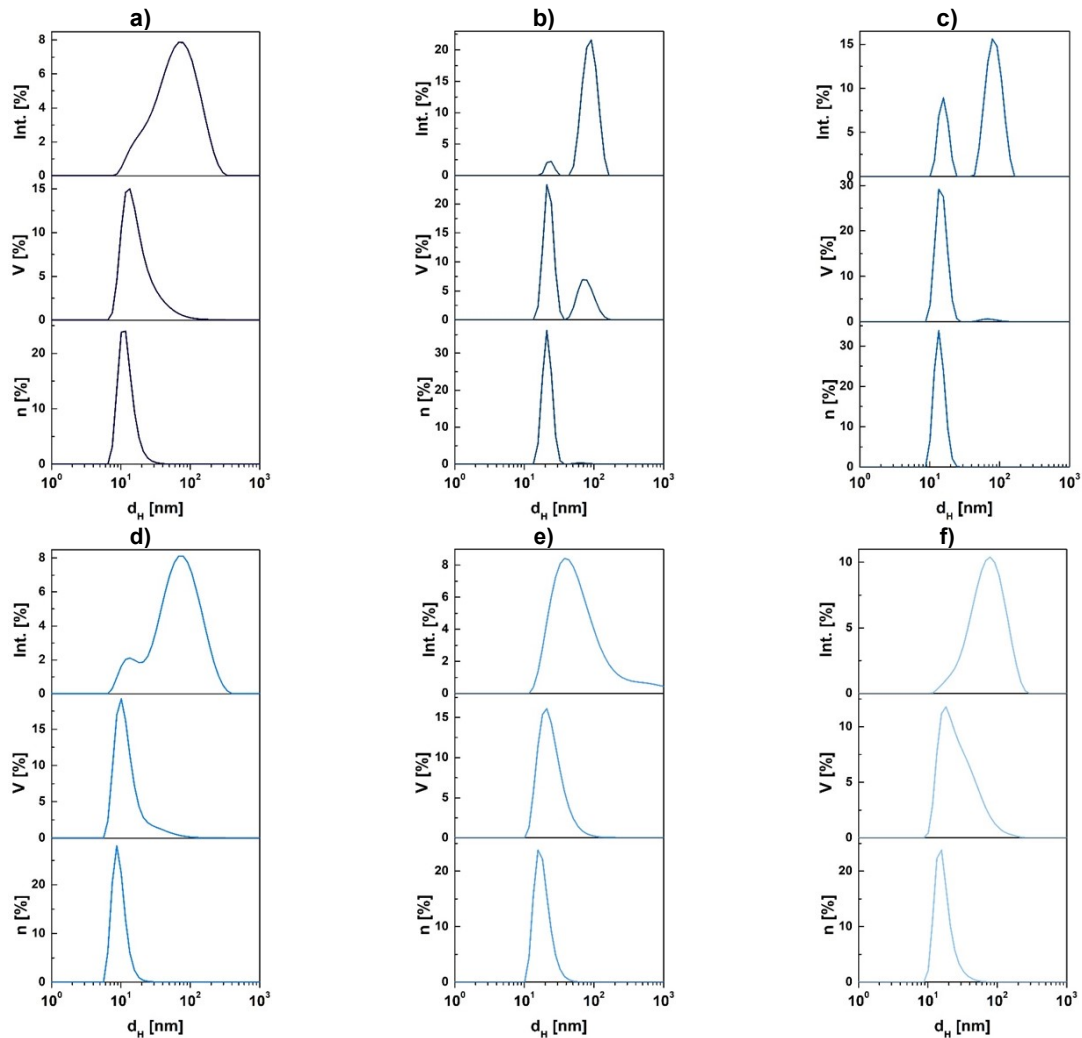


Figure S25. Intensity-averaged, volume-averaged and number-averaged size distribution of solvodynamic diameter of as-prepared of (a) **ZnO-DMSO'**, (b) **ZnO-DBSO'**, (c) **ZnO-TMSO'**, (d) **ZnO-MPSO'**, (e) **ZnO-DPSO'** and (f) **ZnO-DTSO'** obtained from the representative DLS measurements in DMSO.

Nuclear Magnetic Resonance (NMR) spectroscopy

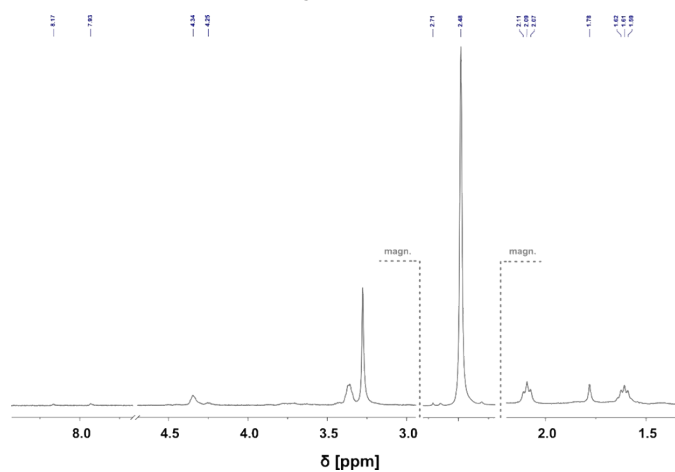


Figure S26. ^1H NMR spectra of $\text{ZnO-DMF}'$ in DMSO-d_6 .

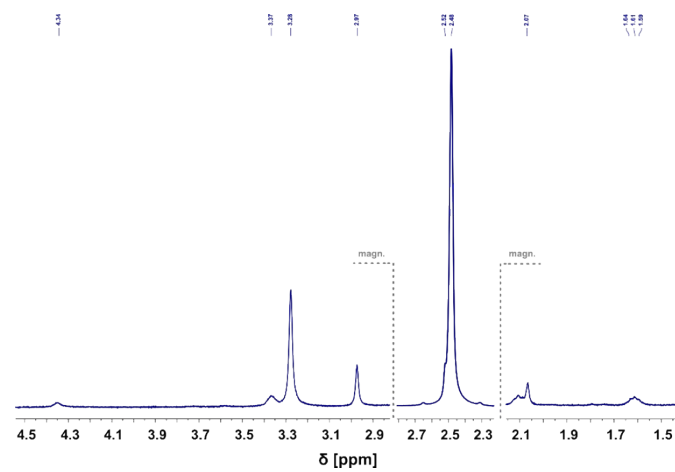


Figure S27. ^1H NMR spectra of $\text{ZnO-DMSO}'$ in DMSO-d_6 .

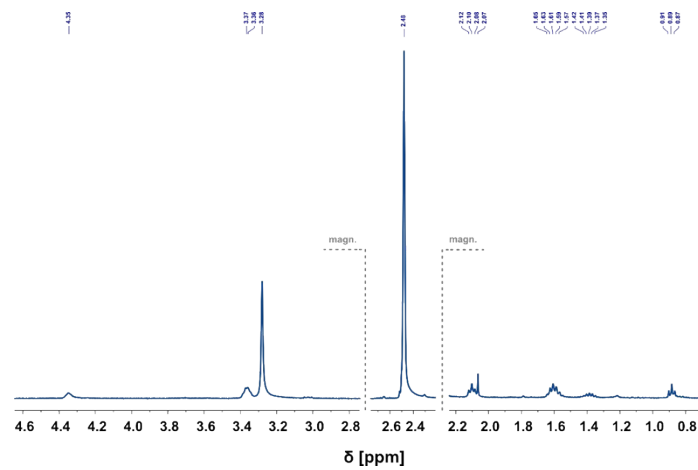


Figure S28. ^1H NMR spectra of $\text{ZnO-DBSO}'$ in DMSO-d_6 .

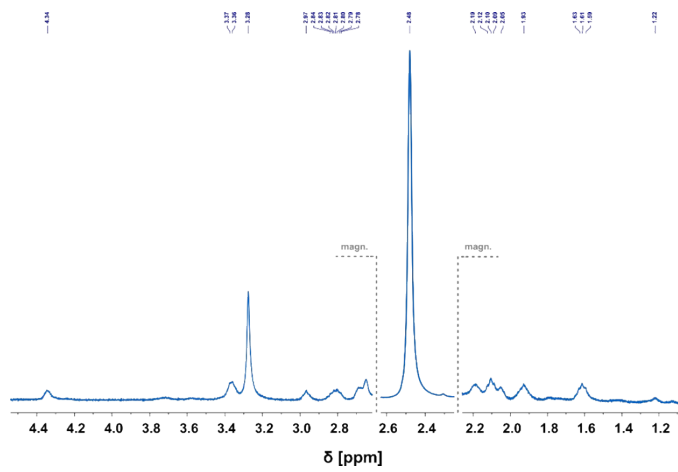


Figure S29. ^1H NMR spectra of ZnO-TMSO' in DMSO-d₆.

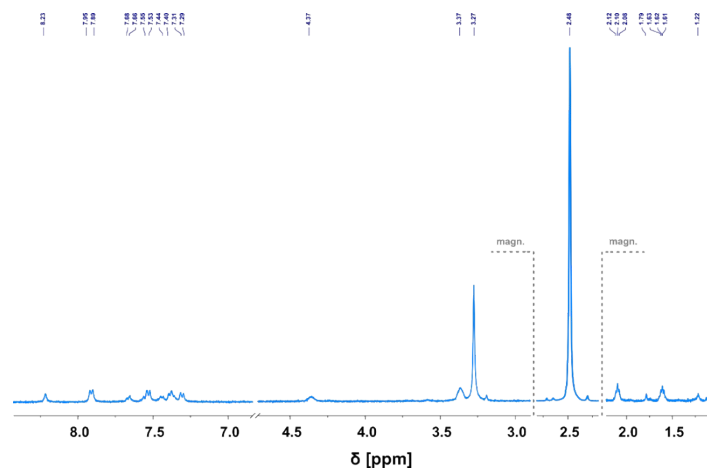


Figure S30. ^1H NMR spectra of ZnO-MPSO' in DMSO-d₆.

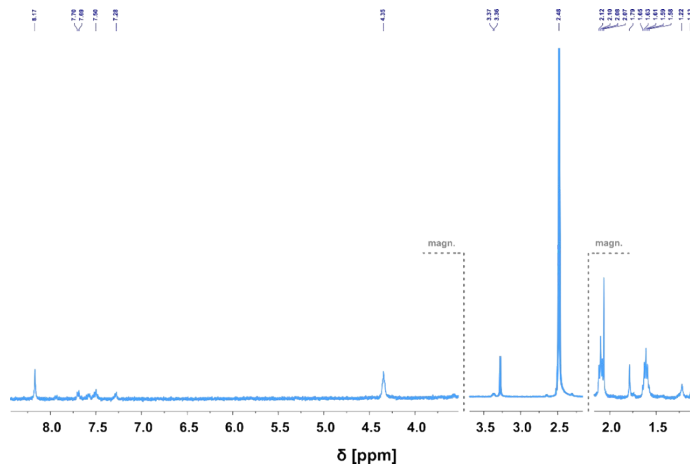
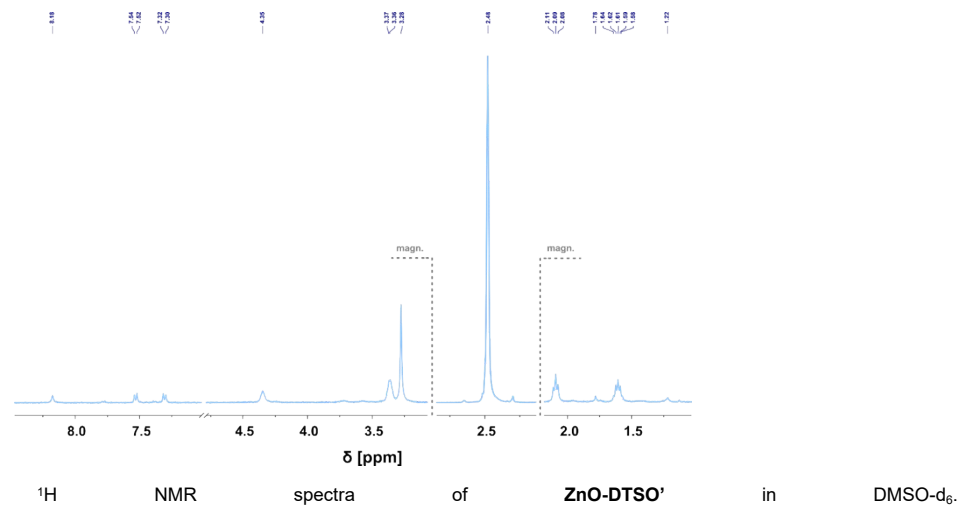


Figure S31. ^1H NMR spectra of ZnO-DPSO' in DMSO-d₆.



Fourier Transform Infrared (FTIR) spectroscopy

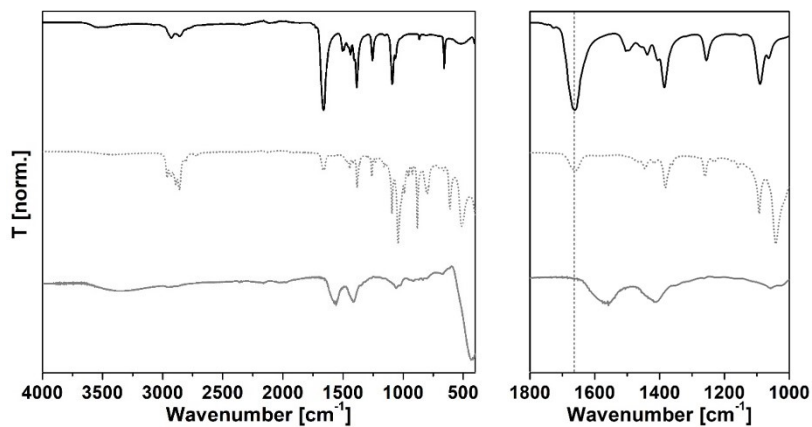


Figure S33. FTIR spectra of $\text{ZnO-DMF}'$ (dark grey line), the corresponding organometallic adduct-type precursor $[\text{Et}_2\text{Zn}(\text{DMF})]_x$ (dotted line) and pure DMF (black line).

DMF: IR (ATR) $\nu = 3539$ (vw), 3482 (vw), 3073 (vw), 2926 (vw), 2856 (vw), 2775 (vw), 2328 (vw), 1726 (vw), 1663 (vs), 1502 (w), 1440 (w), 1385 (s), 1256 (m), 1152 (vw), 1092 (s), 1063 (m), 865 (w), 805 (vw), 658 (m), 518 (w), 404 (w) cm^{-1} .
 $[\text{Et}_2\text{Zn}(\text{DMF})]_x$: IR (ATR): $\nu = 3421$ (vw), 2962 (w), 2933 (w), 2893 (w), 2858 (m), 2806 (vw), 2719 (vw), 2125 (vw), 1920 (vw), 1661 (w), 1445 (vw), 1418 (vw), 1383 (w), 1260 (w), 1229 (vw), 1158 (vw), 1093 (s), 1041 (vs), 989 (m), 958 (w), 924 (w), 881 (vs), 798 (m), 662 (w), 611 (s), 516 (vs) cm^{-1} .

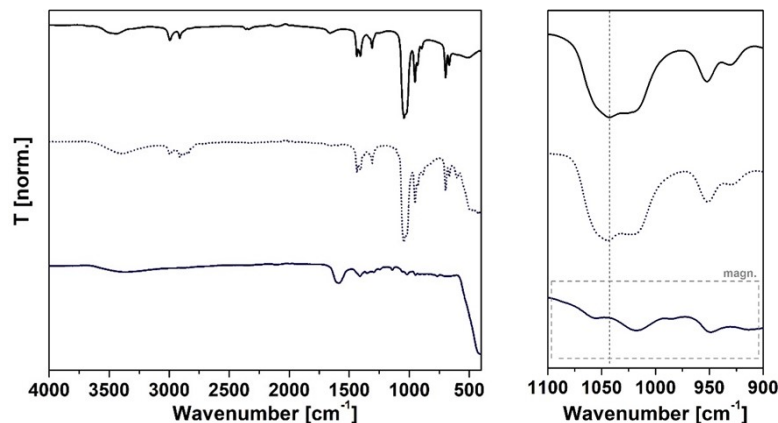


Figure S34. FTIR spectra of $\text{ZnO-DMSO}'$ (blue line), the corresponding organometallic adduct-type precursor $[\text{Et}_2\text{Zn}(\text{DMSO})]_x$ (dotted line) and pure pro-ligand (black line).

DMSO: IR (ATR): $\nu = 3445$ (vw), 2992 (m), 2911 (m), 2822 (vw), 2087 (vw), 1990 (vw), 1954 (vw), 1641 (vw), 1437 (m), 1405 (m), 1333 (vw), 1309 (w), 1293 (vw), 1052 (vs), 1041 (vs), 1031 (vs), 1019 (vs), 953 (m), 930 (w), 894 (vw), 696 (m), 666 (w), 648 (vw), 416 (vw) cm^{-1} .
 $[\text{Et}_2\text{Zn}(\text{DMSO})]_x$: IR (ATR): $\nu = 3394$ (vw), 2995 (vw), 2970 (vw), 2937 (vw), 2911 (vw), 2887 (vw), 2843 (vw), 2809 (vw), 2322 (vw), 1657 (vw), 1601 (vw), 1437 (w), 1406 (w), 1375 (vw), 1332 (vw), 1309 (w), 1228 (w), 1162 (vw), 1134 (vw), 1093 (vw), 1043 (vs), 1019 (vs), 952 (m), 931 (w), 888 (w), 835 (w), 695 (m), 667 (w), 601 (w), 494 (s), 423 (s) cm^{-1} .

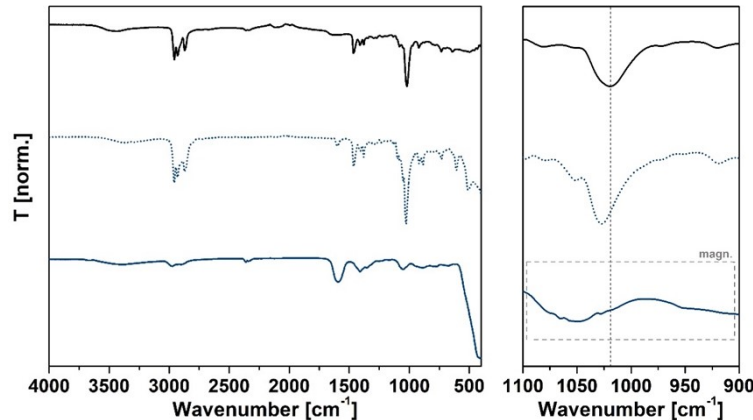


Figure S35. FTIR spectra of ZnO-DBSO' (blue line) the corresponding organometallic adduct-type precursor $[Et_2Zn(DBSO)]_x$ (dotted line) and pure pro-ligand (black line).

DBSO: IR (ATR): $\nu = 3437$ (vw), 2957 (m), 2929 (m), 2869 (m), 2117 (vw), 2085 (vw), 1994 (vw), 1632 (vw), 1581 (vw), 1465 (m), 1409 (w), 1380 (w), 1342 (w), 1295 (w), 1269 (w), 1221 (vw), 1183 (vw), 1132 (vw), 1079 (w), 1019 (vs), 969 (w), 920 (w), 895 (w), 873 (w), 805 (w), 782 (w), 732 (m), 697 (w), 641 (m), 512 (m), 501 (m), 455 (m), 427 (w) cm^{-1}
 $[Et_2Zn(DBSO)]_x$: IR (ATR): $\nu = 3375$ (vw), 3296 (vw), 2958 (m), 2930 (m), 2905 (w), 2872 (w), 2807 (vw), 2726 (vw), 1596 (vw), 1464 (w), 1409 (vw), 1381 (w), 1342 (vw), 1294 (vw), 1272 (vw), 1228 (vw), 1182 (vw), 1131 (vw), 1099 (w), 1078 (w), 1050 (m), 1027 (vs), 972 (w), 949 (w), 918 (w), 885 (w), 807 (vw), 784 (vw), 730 (w), 700 (vw), 634 (w), 606 (w), 510 (s), 454 (m) cm^{-1} .

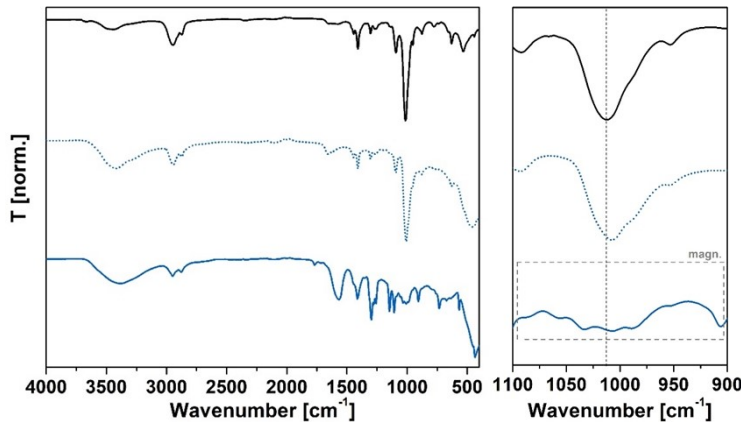


Figure S36. FTIR spectra of ZnO-TMSO' (blue line), the corresponding organometallic adduct-type precursor $[Et_2Zn(TMSO)]_x$ (dotted line) and pure pro-ligand (black line).

TMSO: IR (ATR): $\nu = 3664$ (vw), 3450 (vw), 2943 (w), 2873 (vw), 2359 (vw), 2328 (vw), 2108 (vw), 1901 (vw), 1648 (vw), 1596 (vw), 1445 (vw), 1408 (w), 1305 (vw), 1268 (vw), 1252 (vw), 1148 (vw), 1133 (vw), 1094 (w), 1012 (vs), 951 (w), 892 (vw), 874 (vw), 774 (vw), 734 (vw), 658 (vw), 631 (w), 531 (w), 441 (vw) cm^{-1}
 $[Et_2Zn(TMSO)]_x$: IR (ATR): $\nu = 3419$ (w), 3288 (vw), 2943 (w), 2872 (vw), 2108 (vw), 1659 (vw), 1614 (vw), 1552 (vw), 1460 (vw), 1445 (vw), 1409 (w), 1304 (vw), 1263 (vw), 1145 (vw), 1134 (vw), 1094 (w), 1007 (vs), 953 (m), 889 (w), 877 (w), 781 (w), 770 (w), 658 (w), 630 (m), 529 (s), 461 (vs) cm^{-1} .

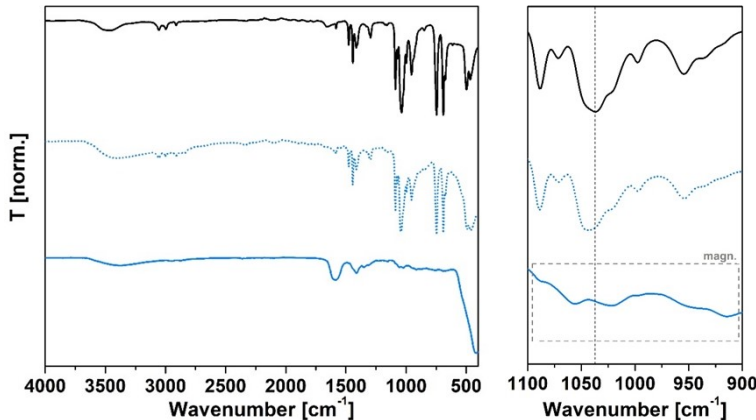


Figure S37. FTIR spectra of ZnO-MPSO' (blue line), the corresponding organometallic adduct-type precursor $[Et_2Zn(MPSO)]_x$ (dotted line) and pure pro-ligand (black line).

(MPSO): IR (ATR): $\nu = 3077$ (w), 3054 (w), 2984 (w), 2903 (w), 1891 (vw), 1816 (vw), 1771 (vw), 1672 (vw), 1607 (vw), 1581 (vw), 1474 (w), 1442 (m), 1420 (w), 1408 (w), 1361 (vw), 1331 (vw), 1303 (w), 1287 (vw), 1172 (vw), 1158 (vw), 1089 (s), 1067 (m), 1033 (vs), 1019 (s), 995 (m), 969 (m), 951 (s), 918 (w), 857 (vw), 745 (vs), 689 (vs), 682 (s), 612 (vw), 491 (s), 467 (s), 406 (vw) cm^{-1}
 $[Et_2Zn(MPSO)]_x$: IR (ATR): $\nu = 3406$ (w), 3162 (vw), 3056 (w), 2996 (vw), 2969 (vw), 2911 (vw), 2879 (vw), 2842 (vw), 2673 (vw), 2356 (vw), 2331 (vw), 2118 (vw), 2085 (vw), 1953 (vw), 1886 (vw), 1812 (vw), 1767 (vw), 1667 (vw), 1602 (vw), 1581 (vw), 1544 (vw), 1500 (vw), 1476 (w), 1442 (m), 1413 (w), 1403 (w), 1368 (vw), 1327 (vw), 1304 (vw), 1295 (w), 1237 (vw), 1174 (vw), 1154 (vw), 1088 (s), 1071 (m), 1043 (vs), (1018 (s), 996 (s), 954 (s), 937 (m), 885 (w), 847 (w), 746 (vs), 690 (vs), 673 (m), 611 (w), 591 (m), 532 (m), 495 (vs), 464 (vs) cm^{-1} .

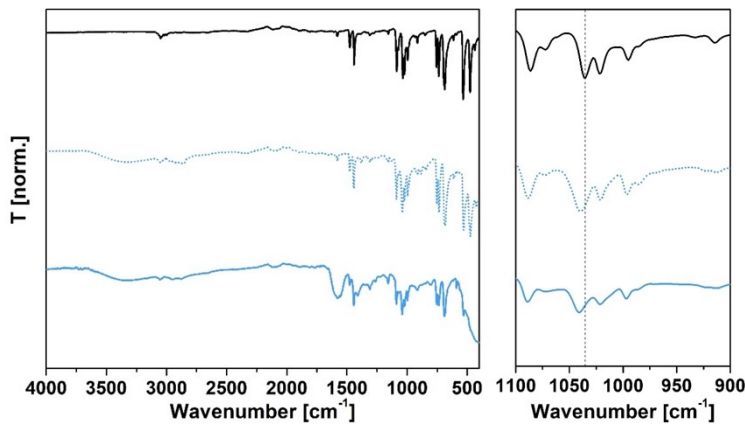


Figure S38. FTIR spectra of ZnO-DPSO' (blue line), the corresponding organometallic adduct-type precursor $[\text{Et}_2\text{Zn}(\text{DPSO})]_x$ (dotted line) and pure pro-ligand (black line).

(DPSO): IR (ATR): $\nu = 3064$ (w), 3052 (m), 3048 (m), 3034 (w), 3018 (w), 2999 (m), 2988 (w), 2900 (w), 2887 (w), 2119 (w), 2068 (w), 1899 (w), 1810 (w), 1609 (w), 1582 (w), 1575 (w), 1474 (s), 1440 (s), 1395 (w), 1377 (w), 1339 (w), 1329 (w), 1312 (w), 1304 (w), 1295 (w), 1275 (w), 1247 (w), 1241 (w), 1225 (w), 1175 (w), 1167 (w), 1155 (w), 1087 (vs), 1071 (m), 1059 (w), 1036 (vs), 1021 (vs), 995 (s), 982 (m), 933 (w), 913 (m), 856 (w), 849 (w), 839 (w), 756 (s), 735 (vs), 693 (vs), 685 (vs), 667 (m), 613 (w), 588 (vw), 563 (vw), 532 (vs), 475 (vs), 435 (w), 417 (vw) cm^{-1} .

[Et₂Zn(DPSO)]_x: IR (ATR): $\nu = 3327$ (vw), 3079 (vw), 3053 (vw), 3036 (vw), 3018 (vw), 2997 (vw), 2965 (vw), 2928 (vw), 2887 (vw), 2855 (vw), 2807 (vw), 2719 (vw), 2657 (vw), 2328 (vw), 2116 (vw), 2086 (vw), 2064 (vw), 2000 (vw), 1986 (vw), 1950 (vw), 1897 (vw), 1880 (vw), 1806 (vw), 1762 (vw), 1705 (vw), 1656 (vw), 1604 (vw), 1577 (vw), 1543 (vw), 1530 (vw), 1477 (w), 1442 (m), 1379 (vw), 1332 (vw), 1307 (vw), 1290 (vw), 1266 (vw), 1234 (vw), 1173 (vw), 1157 (vw), 1129 (vw), 1088 (m), 1073 (w), 1039 (m), 1021 (m), 997 (m), 986 (m), 966 (w), 949 (w), 925 (w), 913 (w), 884 (w), 853 (w), 842 (w), 754 (s), 734 (s), 690 (vs), 682 (vs), 613 (w), 590 (w), 562 (w), 530 (vs), 484 (vs), 474 (w), 424 (s) cm^{-1} .

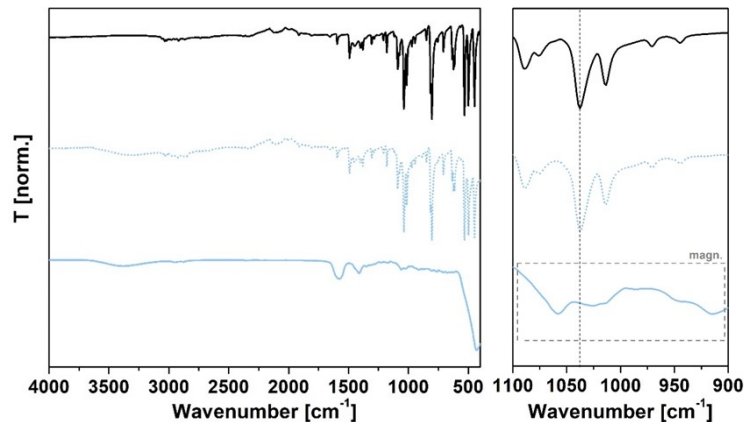


Figure S39. FTIR spectra of ZnO-DTSO' (blue line), the corresponding organometallic adduct-type precursor $[\text{Et}_2\text{Zn}(\text{DTSO})]_x$ (dotted line) and pure pro-ligand (black line).

(DTSO): IR (ATR): $\nu = 3058$ (w), 3035 (m), 3019 (m), 2977 (m), 2949 (m), 2919 (m), 2866 (m), 2739 (w), 2113 (w), 1995 (w), 1915 (w), 1809 (w), 1658 (w), 1650 (w), 1593 (w), 1573 (w), 1491 (m), 1450 (m), 1401 (m), 1380 (m), 1355 (w), 1305 (w), 1285 (w), 1250 (w), 1210 (w), 1179 (m), 1117 (w), 1088 (m), 1074 (m), 1036 (vs), 1013 (s), 971 (w), 943 (w), 849 (w), 813 (s), 803 (vs), 756 (w), 707 (w), 697 (vw), 634 (w), 623 (m), 615 (m), 534 (vs), 498 (s), 447 (vs), 407 (vw) cm^{-1} .

[Et₂Zn(DTSO)]_x: IR (ATR): $\nu = 3320$ (vw), 3057 (vw), 3034 (vw), 3021 (vw), 2973 (vw), 2919 (vw), 2863 (vw), 2737 (vw), 2675 (vw), 2351 (vw), 2328 (vw), 2297 (vw), 2112 (vw), 2087 (vw), 1998 (vw), 1914 (vw), 1808 (vw), 1652 (vw), 1594 (vw), 1574 (vw), 1493 (w), 1452 (w), 1399 (w), 1381 (w), 1356 (vw), 1305 (vw), 1284 (vw), 1246 (vw), 1211 (vw), 1181 (w), 1157 (vw), 1117 (vw), 1088 (m), 1075 (w), 1038 (vs), 1013 (s), 969 (w), 944 (w), 885 (vw), 847 (w), 814 (s), 805 (vs), 756 (w), 708 (w), 698 (w), 680 (vw), 634 (m), 621 (m), 616 (m), 558 (w), 530 (vs), 499 (vs), 444 (vs) cm^{-1} .

Thermogravimetric analysis (TGA)

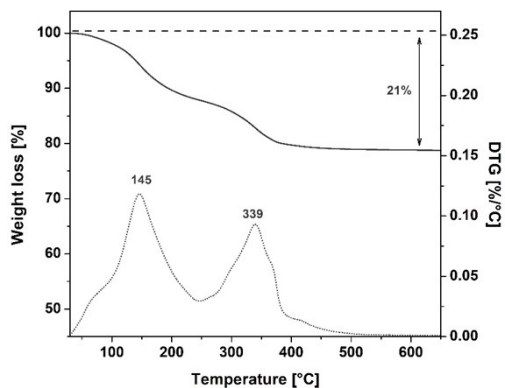


Figure S40. The TGA (solid line) and derivative thermogravimetric analysis (DTG) (dotted line) traces showing the decomposition of **ZnO-DMF'** under synthetic air flow conditions.

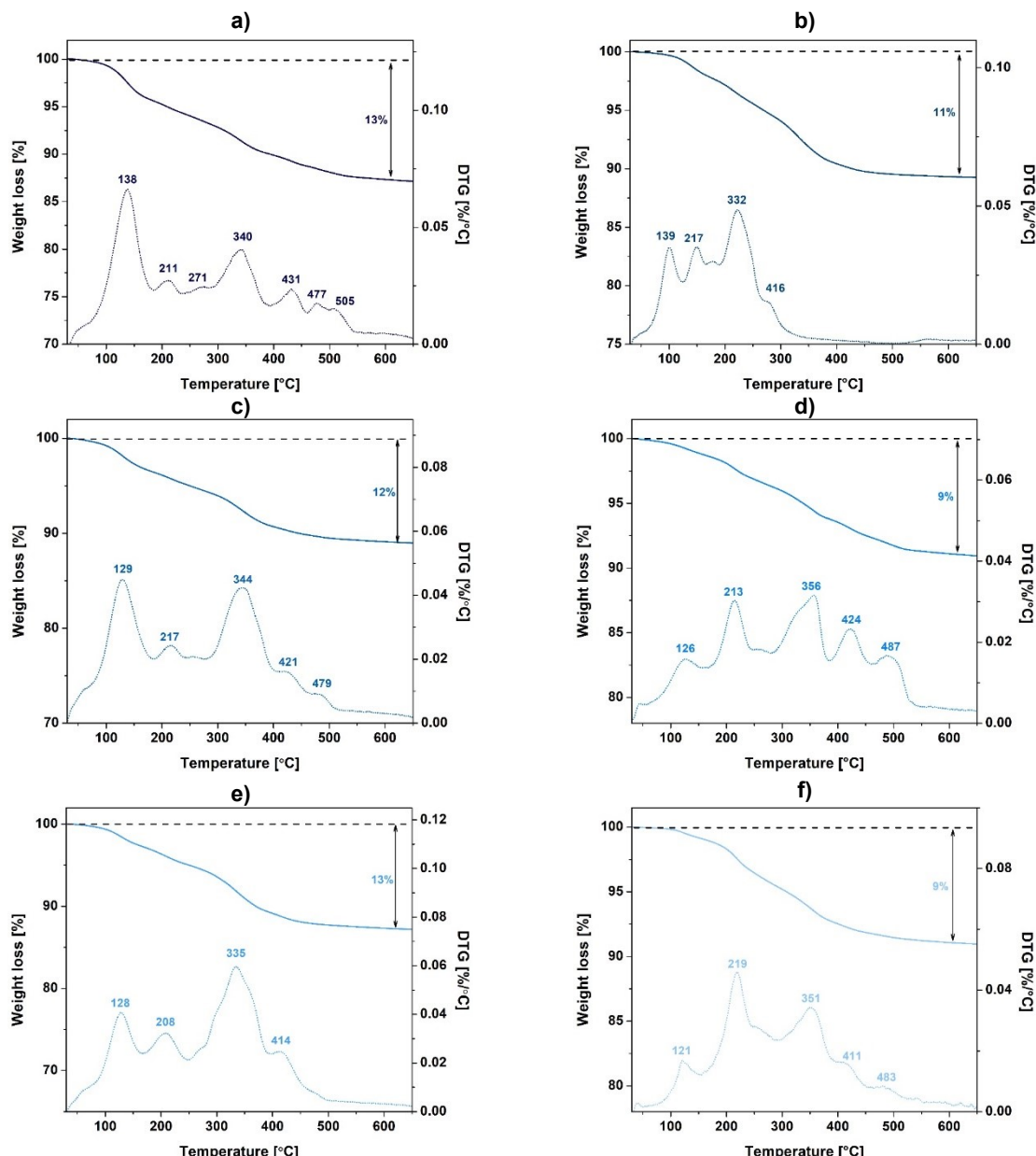


Figure S41. The TGA (solid line) and derivative thermogravimetric analysis (DTG) (dotted line) traces showing the decomposition of (a) **ZnO-DMSO'**, (b) **ZnO-DBSO'**, (c) **ZnO-TMSO'**, (d) **ZnO-MPSO'**, (e) **ZnO-DPSO'** and (f) **ZnO-DTSO'** under synthetic air flow conditions.

5. Additional information and calculations for TGA, DLS and optical data

Ligand content determined from TGA data

The number of bound ligands per unit surface area (i.e., the grafting density, σ) is a critical feature to consider especially in terms of designing functionalized nanomaterials. The relative mass of organic ligand and the mass of the pure ZnO QDs were found from the experimental TGA data. Note that TGA is an effective method which provide insight into the true value of the grafting density as well as the magnitude of the methodological systematic errors.²

Grafting density (σ) was calculated as follows:

$$\sigma = \frac{n_l}{n_{QDs} \times S_{QDs}}$$

where:

n_l – number of ligands attached to ZnO QDs' core

n_{QDs} – number of ZnO cores

S_{QDs} – surface area of spherical QD (πr^2)

$$n_l = \frac{wt\%_l}{m_l} = \frac{wt\%_l \times N_A}{MW_l}$$

$wt\%_l$ – weight loss percentage (from TGA results)

N_A – Avogadro's number

m_l – ligand mass

MW_l – ligand molar mass

$$n_{QDs} = \frac{wt\%_{QDs}}{m_{QDs}} = \frac{wt\%_{QDs}}{\rho_{ZnO} \times V_{QD}}$$

$wt\%_{QDs}$ – weight percentage of the core (100%- $wt\%$)

ρ_{ZnO} – density of bulk ZnO

$$V_{NC} = \frac{4}{3}\pi r^3$$

r – radius of QD

For the determination of ligand coverage (exclusively organic layer) excluding water molecules or hydroxyl groups, the weight loss corresponding to the water content from TGA results has been subtracted from the value applied in equation. Grafting density excluding water content was calculated by modifying the equation as follows:

$$n_l^* = \frac{wt\%_l^*}{m_l} = \frac{(wt\%_l - wt\%_{H2O}) \times N_A}{MW_l}$$

n_l – number of organic ligands attached to ZnO QDs' core

$wt\%_l$ – weight loss percentage (from TGA results)

$wt\%_{H2O}$ – weight loss percentage attributed to water molecules (from TGA results)

$$n_{QDs}^* = \frac{wt\%_{QDs}^*}{m_{QDs}} = \frac{wt\%_{QDs}^*}{\rho_{ZnO} \times V_{QD}}$$

n_{QDs}^* – recalculated number of ZnO cores

$wt\%_{QDs}^*$ – weight percentage of the core (100%- $wt\%_l^*$)

The results from TGA and grafting density calculations for each sample of ZnO QDs are presented in Tables S2-3.

Table S1. The results of TGA measurements and calculated grafting density of ZnO-DMF, ZnO-DBSO and ZnO-DMF'.

Sample name	ZnO-DMF	ZnO-DBSO	ZnO-DMF'
-------------	---------	----------	----------

<i>Ligand coverage</i> [%]	11.7/6.4*	12.3/8.6	21.4
<i>Grafting density</i> [ligand/nm ²]	4/2*	2/2*	7/3*

*value excluding water/OH content

Table S2. The results of TGA measurements and calculated grafting density of sulfoxide-coated ZnO-L QDs.

Sample name	ZnO-DMSO'	ZnO-DBSO'	ZnO-TMSO'	ZnO-MPSO'	ZnO-DPSO'	ZnO-DTSO'
<i>Ligand coverage</i> [%]	12.9/8.5*	11.1/9.1*	11.8/8.3*	9.6/8.3*	13.3/10.6*	9.6/8.8*
<i>Grafting density</i> [ligand/nm ²]	8/5*	3/2*	5/4*	3/2*	3/2*	2/2*

*value excluding water/OH content

DLS results - summary

Table S3. The values of polydispersity index (Pdl) and Z-average of investigated ZnO QDs.

Sample name	ZnO-DMF	ZnO-DBSO	ZnO-DMF'
Pdl	0.488 ¹	0.263 ¹	0.181 ³
Z-average	71.50 ¹	68.76 ¹	1030 ³
ζ -potential [mV] ²	25.2 ± 4.05 ²	26.0 ± 3.87 ²	31.7 ± 4.07 ²

Table S4. The values of polydispersity index (Pdl) and Z-average of investigated ZnO-L QDs.

Sample name	ZnO-DMSO'	ZnO-DBSO'	ZnO-TMSO'	ZnO-MPSO'	ZnO-DPSO'	ZnO-DTSO'
Pdl ¹	0.398	0.149	0.466	0.415	0.284	0.227
Z-average ¹	51.17	75.37	42.70	47.98	45.95	61.30
ζ -potential [mV] ²	36.2 ± 4.0	35.4 ± 4.56	31.5 ± 4.77	31.9 ± 4.34	35.6 ± 4.34	37.2 ± 4.94

Measurements performed in ¹ - DMSO, ² – water.

Optical measurements – summary

All the luminescence decay curves for ZnO QDs are fitted with a fourth-order exponential function described with the following equation:

$$I(t) = A_1 \exp\left(\frac{-t}{T_1}\right) + A_2 \exp\left(\frac{-t}{T_2}\right) + A_3 \exp\left(\frac{-t}{T_3}\right) + A_4 \exp\left(\frac{-t}{T_4}\right)$$

Table S5. PL lifetimes (excitation wavelength – 340 nm) of ZnO QDs performed in the solid state.

Sample name	ZnO-DMF	ZnO-DBSO	ZnO-DMF'	
PL decay time T [ns (% contribution)]	T_1 T_2 T_3 T_4 $\langle T \rangle$	9.8 (80.0) 40.2 (17.8) 254.6 (1.7) 791.1 (0.5) $\langle T \rangle$ $\langle 204.1 \rangle$	28.5 (78.1) 114.5 (12.3) 925.6 (7.6) 3166.1 (2.0) $\langle 1590.2 \rangle$ $\langle 1554.3 \rangle$	21.0 (69.1) 67.8 (22.0) 708.7 (5.9) 2586.4 (3.0) $\langle 1554.3 \rangle$
χ^2		1.15	1.04	1.01

T_{1-n} – PL decay components, $\langle T \rangle$ - mean value of PL decay time.

Table S6. PL lifetimes (excitation wavelength – 340 nm) of ZnO-L QDs performed in the solid state.

Sample name	ZnO-DMSO'	ZnO-DBSO'	ZnO-TMSO'	ZnO-MPSO'	ZnO-DPSO'	ZnO-DTSO'
PL decay time T [ns (% contribution)]	T_1 T_2 T_3 T_4 $\langle T \rangle$	22.6 (70.0) 66.7 (23.6) 674.9 (4.8) 2345.2 (1.6) $\langle 1154.1 \rangle$	27.8 (80.2) 111.3 (11.3) 780.2 (6.0) 2875.8 (2.5) $\langle 1586.8 \rangle$	20.2 (61.9) 58.9 (29.5) 743.3 (6.8) 2649.1 (1.8) $\langle 1283.3 \rangle$	18.9 (65.1) 62.1 (26.9) 712.9 (5.7) 2604.7 (2.3) $\langle 1424.1 \rangle$	24.7 (73.4) 77.8 (17.6) 751.8 (6.5) 2731.9 (2.5) $\langle 1506.4 \rangle$
χ^2		1.03	0.95	1.06	0.93	1.01
						0.95

*Gauss fitting, T_{1-n} – PL decay components, $\langle T \rangle$ – mean value of PL decay time.

6. References

- 1 Z. Zhao, Z. Zheng, C. Roux, C. Delmas, J.-D. Marty, M. L. Kahn and C. Mingotaud, *Chem. Eur. J.*, 2016, **22**, 12424–12429.
- 2 D. N. Benoit, H. Zhu, M. H. Lilierose, R. A. Verm, N. Ali, A. N. Morrison, J. D. Fortner, C. Avendano and V. L. Colvin, *Anal. Chem.*, 2012, **84**, 9238–9245.